Magnetic Resonance in Medicine 58:725–734 (2007)

Fluorine-19 MRI for Visualization and Quantification of Cell Migration in a Diabetes Model

Mangala Srinivas,[1] Penelope A. Morel,[2] Lauren A. Ernst,[3] David H. Laidlaw,[4] and Eric T. Ahrens[1,5]*

This article describes an in vivo imaging method for visualizing and quantifying a specific cell population. Cells are labeled ex vivo with a perfluoropolyether nanoparticle tracer agent and then detected in vivo using ^{19}F MRI following cell transfer. ^{19}F MRI selectively visualizes only the labeled cells with no background, and a conventional ^{1}H image taken in the same imaging session provides anatomical context. Using the nonobese diabetic mouse, an established model of type 1 diabetes, ^{19}F MRI data were acquired showing the early homing behavior of diabetogenic T cells to the pancreas. A computational algorithm provided T cell counts in the pancreas. Approximately 2% of the transferred cells homed to the pancreas after 48 hr. The technique allows for both unambiguous detection of labeled cells and quantification directly from the in vivo images. The in vivo quantification and cell trafficking patterns were verified using ^{19}F spectroscopy and fluorescence microscopy in excised pancreata. The labeling procedure did not affect T-cell migration in vivo. This imaging platform is applicable to many cell types and disease models and can potentially be used for monitoring the trafficking of cellular therapeutics. Magn Reson Med 58: 725–734, 2007. © 2007 Wiley-Liss, Inc.

Key words: T cells; diabetes; MRI; cell tracking; fluorocarbon

A common characteristic of autoimmune disease is an inappropriate trafficking of immune cells into tissues. Type 1 diabetes (T1D) is a common autoimmune disease characterized by the destruction of the insulin-producing β cells of the islets of Langerhans. Prior to the development of diabetes, the islets become heavily infiltrated with lymphoid cells, including CD4+ and CD8+ T cells, dendritic cells, and monocytes (1). By the time diabetes appears, over 90% of the islets have been destroyed by these infiltrates. The nonobese diabetic (NOD) mouse is a widely studied model of human T1D and shares many of the genetic and immunological features of the human disease (2). The ability to noninvasively image the trafficking patterns of phenotypically defined populations of immune cells would be of tremendous benefit to animal model studies, such as in the NOD mouse. Imaging immune cells in the early and late phases of T1D is important to understand the pathogenesis of autoimmunity and for designing immunotherapeutic interventions. These capabilities may permit longitudinal migration studies and the ability to noninvasively assay the efficacy of trial therapies.

Numerous studies have investigated the feasibility of in vivo MRI cell tracking of various cell types labeled ex vivo with paramagnetic contrast agents (for example, see Refs. 3–9). Superparamagnetic iron-oxide (SPIO) nanoparticle contrast agents have been used to track autoreactive T-cell migration (10–12). In the NOD mouse, islet transplantation and pancreatic inflammation have been visualized in vivo using SPIO agents (13–15).

Cell labeling using metal-ion-based paramagnetic contrast agents often have the advantage of high sensitivity in certain tissues. For example, in vivo detection of single-labeled cells has been reported by several groups (16,17). However, intracellular labeling with paramagnetic agents also may present several challenges, including the task of discriminating labeled cells from the image background and biocompatibility concerns. Often these methods require image interpretation of subtle contrast or relaxivity changes in regions believed to contain the labeled cells, making positive identification difficult, perhaps necessitating prescans or prior knowledge of the cell biodistribution. Image interpretation can be further confounded by sources of intrinsic contrast or relaxation rate changes among tissues or lesions resulting in false-positives or -negatives. Moreover, quantification of cell numbers in regions of interest (ROIs) is challenging because several subject-dependent parameters must be determined, such as the agent's relaxivity in the specific tissue and individual variability in the background relaxation rate in the ROI. Moreover, the biological impact of the by-products of lysosomal degradation of the metal-ion agents requires careful consideration and characterization.

In this article we describe a cellular MRI method in which we label T cells ex vivo with a novel perfluoropolyether (PFPE) nanoparticle composition, introduce labeled cells into a subject, and monitor cell migration in vivo using spin density-weighted ^{19}F MRI. The key advantage of this approach is that the ^{19}F images are extremely selective for the labeled cells (18). In addition, coregistered conventional proton MR images acquired in the same imaging session place the labeled cells into their anatomical context (18). PFPE is not degraded in vivo and has no known intracellular biological reactivity. Importantly, we show

[1]Department of Biological Sciences, Carnegie Mellon University, Pittsburgh, Pennsylvania.

[2]Department of Immunology, University of Pittsburgh School of Medicine, Pittsburgh, Pennsylvania.

[3]Molecular Biosensor and Imaging Center, Carnegie Mellon University, Pittsburgh, Pennsylvania.

[4]Department of Computer Science, Brown University, Providence, Rhode Island.

[5]Pittsburgh NMR Center for Biomedical Research, Carnegie Mellon University, Pittsburgh, Pennsylvania.

Grant sponsor: National Institutes of Health; Grant numbers: R01-EB003453; R01-EB004155; P01-HD047675; P50-ES012359; Grant sponsor: Pittsburgh NMR Center supported by the National Institute of Biomedical Imaging and Bioengineering as a National Biomedical Research Resource Center; Grant number: P41EB-001977.

*Correspondence to: Eric T. Ahrens, Department of Biological Sciences, Carnegie Mellon University, 4400 Fifth Ave., Pittsburgh, PA 15213. E-mail: eta@andrew.cmu.edu

Received 16 November 2006; revised 28 February 2007; accepted 7 June 2007.

DOI 10.1002/mrm.21352
Published online in Wiley InterScience (www.interscience.wiley.com).

that the absolute number of labeled cells can be estimated directly from the in vivo ^{19}F images, thus providing a unique biomarker.

We applied the PFPE ^{19}F imaging platform to visualize and quantify autoreactive T cells in the pancreas during the early stages of insulitis in the NOD model. We used purified T cells from NOD BDC2.5 transgenic T-cell receptor (TCR) mice (19). All T cells were $CD4^+$ and recognize a pancreatic β islet granule antigen (19). We transferred PFPE-labeled T cells into the peritoneum of major histocompatability complex (MHC) matched host mice and used in vivo ^{19}F MRI to visualize the T cells as they homed to the pancreas. T-cell migration into the pancreas is thought to be one of the earliest events in T1D pathogenesis and is asymptomatic because it occurs long before widespread islet destruction. We quantified the apparent number of T cells migrating to the pancreas directly from the in vivo MRI dataset. High-resolution ^{19}F NMR spectroscopy in excised pancreata validated the cell quantification results. Histological analysis of the pancreas identified the transferred ^{19}F-labeled T cells in and around islets, suggesting specific homing to the islets and appropriate in vivo functionality of the labeled cells. Our results suggest that the PFPE imaging platform is a powerful in vivo cellular MRI technique that can be readily adapted to a wide range of cell and disease model types.

MATERIALS AND METHODS

Label Synthesis and Characterization

PFPE emulsions were prepared using a 1:1 molar ratio of autoclaved perfluoropolyethelene glycol (molecular weight ≈1750, Exfluor, Round Rock, TX) and sterile filtered Pluronic (Sigma-Aldrich, St. Louis, MO). Emulsification was by probe sonication using a Sonifier Cell Disruptor (Misonix, Farmingdale, NY). The average emulsion particle diameter was determined to be 103 ± 4 nm by dynamic light scattering using a Malvern Zetasizer Nano ZS instrument (Malvern Instruments, Worcestershire, UK). Fluorescent PFPE emulsion particles were prepared by mixing 2 μL PFPE emulsion, 1 μg dialkylcarbocyanine dye (DiI, Molecular Probes-Invitrogen, Carlsbad, CA) dissolved in dimethyl sulfoxide (1 μL), 8 μL FuGENE 6 (Invitrogen), and 100 μL Roswell Park Memorial Institute (RPMI) media.

T cell Purification, Activation, and Labeling

T cells from the BDC2.5 TCR transgenic mouse were purified from single-cell suspensions of splenocytes using a magnetic cell sorting (MACS) pan T-cell isolation kit (Miltenyi Biotec, Auburn, CA). Cell were grown in RPMI with 10% fetal bovine serum (FBS; Gibco, Carlsbad, CA), 100 μg/mL each of streptomycin and penicillin, and 1 μL/mL of 2-mercaptoethanol. Cells were activated in vitro by a 3-day incubation on plates coated with anti-TCR antibody in the presence of 1 μg/mL anti-CD28 and 10 U/mL IL-2. Cells were then harvested and resuspended in fresh medium at 2×10^6 /mL. The PFPE emulsion (2 μL) was premixed with 8 μL of FuGENE 6 (Roche, Indianapolis, IN) transfection agent in 300 μL FBS-free media for 20 min; this mix was added to the cell suspension at 2 μL/mL and incubated for 3.5 hr. Cells were washed in phosphate-buffered saline (PBS) twice and resuspended in 300 μL Hank's balanced salt solution (HBSS) prior to inoculation. Alternatively, electroporation cell labeling was carried out on aliquots of 5×10^6 T cells in HBSS. A unidirectional 80 mV pulse of 20 ms length was delivered via a BTX 830 electroporator (Harvard Apparatus, Holliston, MA). Cells were then incubated on ice for 10 min before the addition of media and a further incubation of 4 hr at 37°C.

Cellular Toxicity, Proliferation, and Phenotype

Cellular viability was measured using the methyl thiazole tetrazolium (MTT) assay (ATCC, Manassas, VA) according to the manufacturer's instructions. Cell aliquots were assayed at 2, 4, and 48 hr after labeling. Cellular toxicity of labeled cells was also assessed using a Trypan blue exclusion assay; aliquots of cells were mixed with Trypan blue and then counted in a hemocytometer. For the fluorescence activated cell sorting (FACS) analyses, cells were stained using either fluorescein isothiocyanate (FITC) or phycoerythrin (PE) conjugated antibodies against CD4 and CD62L (PharMingen, San Diego, CA). The expression levels of these markers were determined by flow cytometry on a LSRII FACS instrument (Becton Dickinson, Mountain View, CA).

Murine Diabetes Model

Experiments were carried out in accordance with the guidelines provided by the Carnegie Mellon Institutional Animal Care and Use Committee (IACUC) and the National Institutes of Health *Guide for the Care and Use of Laboratory Animals*. NOD SCID and BALB/c mice were obtained from Jackson Laboratories (Bar Harbor, ME) and NOD BDC2.5 mice were bred in-house. All mice were housed in the animal facilities at the University of Pittsburgh or at the Pittsburgh NMR Center for Biomedical Research at Carnegie Mellon University. For the adoptive transfer experiments, purified T cells from the spleens of NOD BDC2.5 mice were activated in vitro, labeled, and transferred intraperitoneally (i.p.) into host NOD SCID mice. Recipient mice were pretreated i.p. with 200 mg/kg of cyclophosphamide (Sigma-Aldrich) in PBS 24 hr before cell transfer (20). All mice were 8–10 weeks old, and each mouse received $2–6 \times 10^6$ labeled cells i.p.

In vivo control experiments were carried out in exactly the same manner, except mice received either cell-free PFPE in HBSS at a ^{19}F dose equivalent to $\approx 1 \times 10^7$ labeled T cells, or received labeled, activated T cells from MHC-mismatched BALB/c mice in place of the BDC2.5 T cells.

Optical Microscopy

In vitro activated T cells were incubated with the fluorescent emulsion preparation (described above) and washed twice. T cells were incubated on poly-L-lysine-coated glass coverslips for 30 min and then fixed in 1% paraformaldehyde (PFA). The fixed cells were mounted in VectaShield (Vector Laboratories, Burlingame, CA) mounting medium with a 10 μg/mL TOTO-3 nuclear stain (Molecular Probes-Invitrogen) after RNAse treatment. The

slides were then imaged using a Leica TCS SP2 spectral confocal microscope (Leica Microscopes, Exton, PA).

Histological sections were also prepared of the pancreas from NOD SCID mice that had received PFPE-labeled NOD BDC2.5 T cells. The mouse was perfused with 2% PFA 48 hr after cell transfer and its pancreas was excised and immersed in 2% PFA. Frozen sections (6 μm) were mounted on glass slides, stained, and viewed in an Olympus BX51 microscope (Olympus America, Center Valley, PA). Cell nuclei were stained using 4′-6-Diamidino-2-phenylindole (DAPI) and actin was stained with phalloidin. T cells were immunostained using rat antimouse CD4 primary (PharMingen-BD Biosciences, San Jose, CA) and goat antirat Cy3 secondary antibodies (Jackson ImmunoResearch Laboratories, West Grove, PA). Insulin was stained using an anti-insulin rabbit polyclonal (Santa Cruz Biotechnology, Santa Cruz, CA) and goat antirabbit Cy5 secondary antibodies (Jackson ImmunoResearch Laboratories).

NMR

All ^{19}F NMR measurements were made at 470 MHz using a Bruker DRX500 spectrometer (Bruker BioSpin, Billerica, MA). The mean intracellular ^{19}F dose per cell, F_c, was measured by pelleting 1×10^6 labeled cells in an NMR tube. The NMR tube also contained a small sealed capillary containing 5 μL of 5% v/v trifluoroacetic acid (TFA), providing a calibrated quantity of ^{19}F spins. The F_c was calculated from the ratio of the integrated areas of the PFPE and the TFA spectra. For whole organ NMR, mice were sacrificed immediately after MRI and the organs were harvested and fixed with 4% PFA for 48 hr. The fixed organs were placed in NMR tubes that also contained a sealed capillary containing the TFA ^{19}F reference solution. All ^{19}F spectra, except where noted, were acquired using a recycle delay of 8 sec, a 12-μs pulse width, a spectral width of 20 kHz, 2048 acquisition points, and a 90° flip angle.

MRI

Before imaging, mice were anesthetized with a ketamine/xylazine cocktail and an i.p. catheter was secured with sutures and connected to a syringe pump to infuse additional cocktail into the mice for the duration of the experiment. The imaging session lasted ≈2-3 hr, which included the time to prepare, position the mouse, and the actual imaging. A maximum total dose of ≈0.33 mg ketamine and 0.02 mg xylazine was delivered via an incremental step-down dose protocol. During the scan the mouse was intubated and connected to a mechanical ventilator (Harvard Apparatus, Hilliston, MA) delivering 2:1 O_2/NO_2. Mice were positioned in a cradle and imaged using an 11.7T, 89 mm vertical-bore micro-imaging system (Bruker). A volume birdcage-type resonator was used that could be tuned to either 470 MHz for ^{19}F or 500 MHz for ^1H. The mouse temperature was maintained at 35–37°C using a water-filled jacket surrounding the animal cradle that was connected to a regulated closed-cycle water bath. A sealed tube containing dilute PFPE emulsion was placed by the torso in the image field of view and served as a calibrated external ^{19}F reference. ^{19}F images were acquired using a rapid acquisition with relaxation enhanced (RARE) sequence with a RARE factor equal to eight, TR/TE = 1000/6.4 ms, 64×32 image points, a 50 kHz bandwidth, and 1024 signal averages. ^1H images were acquired using a 2DFT spin-echo sequence with TR/TE = 1200/22 ms and 512×256 image points. Eight contiguous, 2-mm thick slices through the torso were acquired for both ^{19}F and ^1H with exactly the same coordinates. The field of view was 5.0×2.8 cm for all acquisitions. All MRI excitations were respiratory-gated.

To validate the MRI cell quantification method, we constructed a phantom containing 5-mm capillaries with different densities of labeled T cells suspended in 2% agarose in PBS. The cell densities used were 87.0, 43.5, 21.9, 10.8, and 5.4 cells/nL, which correspond to 12, 6, 3, 1.5, and 0.75 ($\times 10^4$) cells/voxel, respectively. A ^{19}F reference capillary of dilute emulsion was also placed in the phantom, as is used for the in vivo imaging, except this reference was 4-fold more concentrated to accommodate the higher cell densities used in the phantom. All capillaries were embedded in agarose, and imaging was performed at 37°C using the same birdcage resonator and pulse sequence parameters that were used for the in vivo imaging.

Cell Quantification Using MRI

The quantity of apparent PFPE-labeled cells was calculated directly from the in vivo MRI dataset, the external ^{19}F reference, and the measured F_c. The calculation was performed on a per-slice basis. The noise magnitude, N, of the ^{19}F image was determined by calculating the standard deviation of voxel values near the periphery of the image. The N can be calculated equivalently from either the real or imaginary component. Next, the magnitude values were calculated for each voxel and then corrected to compensate for the resulting Rician-distributed noise that is observed in low signal-to-noise ratio (SNR) images (21). Our Rician correction reset the magnitude value, m, to a lower value, m', such that the expected value of the magnitude of $(m' + 0\ i)$ with noise N added to each component of m' is $m = \mathrm{E}(|\ (m' + n_1) + n_2\ i\ |)$, where E denotes expected value, and n_1 and n_2 are normally distributed random variables with zero mean and standard deviation N. The m can be estimated statistically for a given m' by finding the mean value of m for a set of random values of n_1 and n_2. Random pairs of n_1 and n_2 (1,000,000 trials) were drawn for each estimate of m. To avoid this calculation for each pixel value, m was estimated for $m' = 0, 0.1N, 0.2N, \ldots 8N$. The m' is monotonic in m, thus additional m values were calculated by interpolating the m' results using the Matlab function interp1(). Above $8N$ no adjustment was made because the Rician distribution is approximately Gaussian and the correction was insignificant. Next, the average magnitude signal value, R, was calculated in an ROI containing the ^{19}F reference. The R was calculated by interactively choosing a box containing the reference and automatically identifying voxels within it with magnitude $>2.5N$, thereby setting a confidence factor of >99% that the voxels scored contain actual ^{19}F signal. This automatically calculated ROI was then dilated by ½ voxel in-plane to capture any nearby signal and account for partial vol-

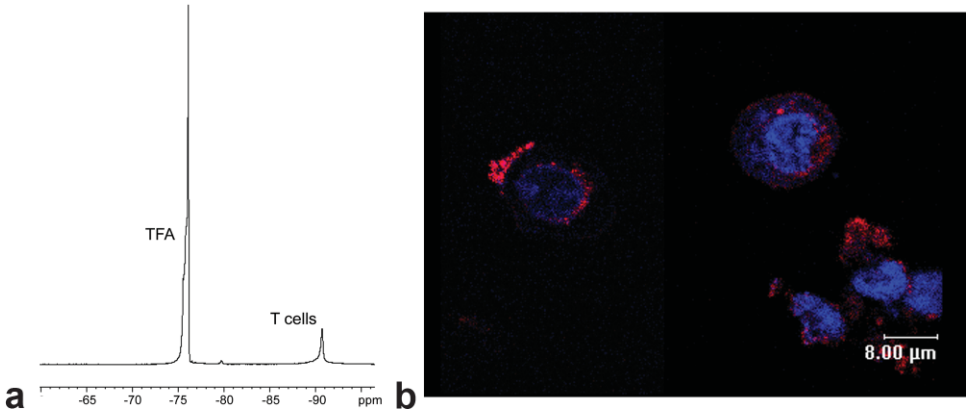

FIG. 1. T cells are efficiently labeled with PFPE nanoparticles ex vivo. (**a**) A ^{19}F NMR spectrum of pelleted, labeled (1×10^6) T cells. The PFPE has two peaks, one at −92 ppm and the other at −79 ppm. A capillary containing trifluoroacetic acid (TFA) was used as a reference alongside the cell pellet and shows a peak at −76 ppm. The ^{19}F NMR was measured at 470 MHz. (**b**) Confocal fluorescence micrographs of labeled, activated T cells. The PFPE nanoparticles were treated with DiI (pink) before cell labeling. Cell nuclei are TOTO3 stained (blue), which also weakly stains the cytoplasm. Nanoparticles are visible both on the cell surface and intracellularly. Scale bar = 8 µm.

ume effects. From this analysis we also calculated a parameter, r, which is the amount of ^{19}F per voxel in the reference. Next, the total signal in the pancreas, P, was calculated. An ROI was defined by interactively choosing a box containing the pancreas, and voxels with signal $>2.5N$ were automatically identified in the magnitude images. Again, the identified region's periphery was dilated by 1/2 voxel. The P was then calculated by summing the adjusted magnitude-valued signal from all of the identified voxels. The number of apparent cells contained in the pancreas, C, was calculated using the relationship $C = (Pr)/(RF_c)$. The uncertainty in C was estimated by using the equation $\sigma(P)r/(RF_c)$, where $\sigma(P) = N\sqrt{2n}$, i.e., the standard deviation of P, and n is the number of voxels identified as having signal. This cell quantification algorithm was also tested on the calibrated phantom containing capillaries with different known densities of labeled T cells suspended in agarose.

RESULTS

Intracellular ^{19}F Labeling

Figure 1 shows a ^{19}F NMR spectrum of activated, labeled T cells. The spectrum of the linear PFPE molecule has two peaks, a major CF_2 peak at −92 ppm and a minor peak at −79 ppm from the CF_2 end groups. The ratio of the spectral weight of these peaks is 10:1, and generally the minor peak is below MRI detectability in vivo. The third peak, at −76 ppm, is from the TFA reference in the sealed capillary. We calculated the mean ^{19}F content per cell (F_c) to be 2.2×10^{13} fluorine atoms postlabeling. Confocal microscopy of the labeled cells confirmed that the PFPE label distribution is intracellular (Fig. 1b).

T cell Viability and Phenotype

To confirm viability and phenotype of labeled T cells, we performed several in vitro assays. Labeled cell viability, assayed immediately after labeling, showed 94 ± 3.7% viability relative to untreated controls, where the error bar is the standard deviation for $n = 6$ wells; at 48 hr postlabeling, the cells displayed 95 ± 6% viability ($n = 3$). We also performed the Trypan blue exclusion assay to confirm minimal cytotoxicity due to labeling (data not shown). To confirm that the labeling process itself does not activate T cells, we studied expression of the cell surface markers CD62L and CD4 on naïve BDC2.5 T cells after labeling. CD62L, a lectin-binding protein that aids in lymphocyte rolling, is expressed at high levels only on naïve T cells. We found minimal downregulation in the expression of CD62L in labeled cells compared to unlabeled cells (Fig. 2a), indicating that labeling does not activate naïve T cells. CD4, a coreceptor that interacts with the MHC II molecule, is expressed on both naïve and activated T cells. The level of CD4 expression was reduced immediately after labeling using the transfection agent, but recovered within 24 hr (Fig. 2b). To better understand the origin of this transient downregulation, T cells were labeled via electroporation, without transfection agent. There was no reduction in CD4 expression immediately after labeling using electroporation (Fig. 2c), indicating that this effect is likely an artifact from transfection agent usage.

In Vivo T cell Homing: Histology

To confirm that the labeling procedure did not interfere with the ability of the T cells to home to the pancreas, we examined histological sections of the pancreas using fluorescence microscopy. For all in vivo experiments we used an established adoptive transfer method that has been shown to result in reproducible diabetes induction (22,23). The BDC2.5 T cells ($\approx 4 \times 10^6$) were purified, activated in vitro, PFPE-labeled, and injected i.p. into a recipient NOD SCID mouse. Figure 3 shows histological sections of the pancreas 48 hr after cell transfer; T cells (red) concentrated around the islets (green), which is consistent with the early stages of insulitis. This result suggests that the PFPE labeling does not interfere with cell homing in vivo, and that the labeled T cells are able to home to the pancreas.

In Vivo T cell Homing: MRI

We next determined whether T-cell homing to the pancreas could be detected using MRI. We performed in vivo MRI experiments in the NOD SCID model, in which purified diabetogenic T cells were activated, labeled, and transferred i.p. into NOD SCID mice as above. We imaged the mice 48 hr posttransfer. A representative ^{19}F/^{1}H composite image is shown in Fig. 4a. The anatomical T_2-weighted ^{1}H image (grayscale) that serves as an underlay was acquired with the same slice geometry and in the same imaging session as the ^{19}F. The ^{19}F images through the torso show localized signal in a region consistent with the pancreas (pseudo-color, Fig. 4a). No ^{19}F was detected in the liver or spleen in the MR images.

To confirm that the detected signal was due to specific T cell homing, we carried out two control in vivo MRI experiments in the NOD model. These employed i.p. injections of either cell-free PFPE nanoparticles or nonspecific, labeled T cells. Imaging results after 48 hr (Fig. 4b) show ^{19}F accumulation from cell-free PFPE in the abdominal cavity near the bladder; no ^{19}F is visible in the pancreas. The second control employed purified nonspecific CD4^{+} T cells from MHC-mismatched BALB/c mice. Since T cells recognize antigen in the context of the MHC, BALB/c T cells are not expected to carry out specific homing in NOD mice. Figure 4c shows that after 48 hr no ^{19}F was detected in or around the pancreas.

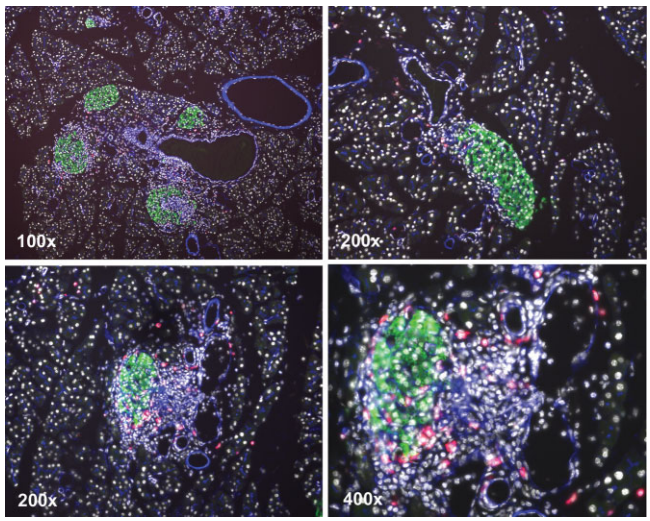

FIG. 3. Fluorescence micrographs of histological sections of pancreatic tissue from a NOD SCID mouse receiving PFPE-labeled T cells. Mice received 4×10^6 labeled BDC2.5 T cells 48 hr prior. The fixed section staining is as follows: insulin is stained green, nuclei white, actin blue, and T cells red. The images show early insulitis, with T cells infiltrating into the islets or around blood vessels, suggesting that PFPE labeling does not impair T cell trafficking.

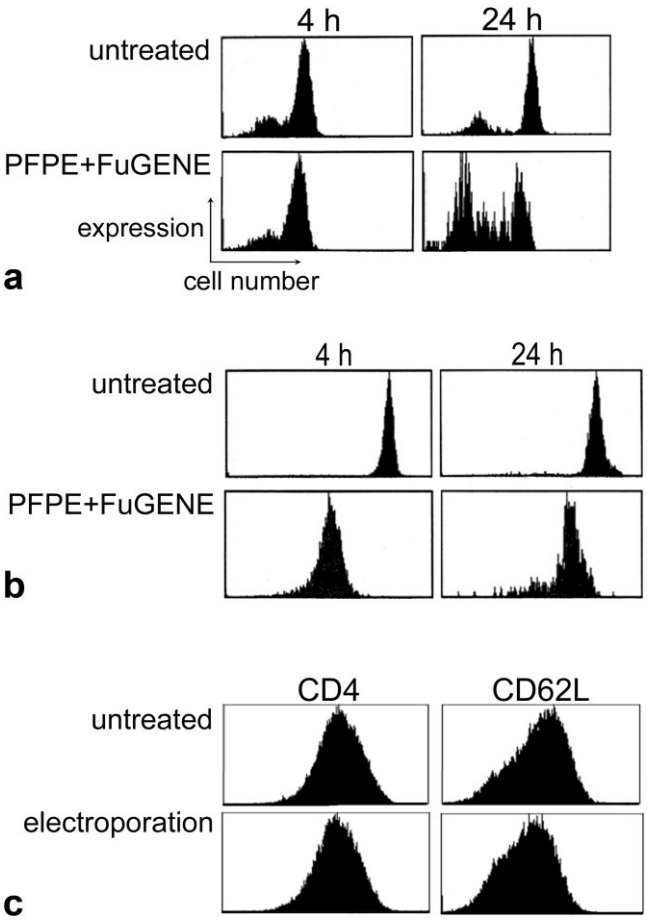

FIG. 2. FACS results in PFPE-labeled T cells. Panels (**a**) and (**b**) are CD62L and CD4 expression levels, respectively, at 4 and 24 hr postlabeling using the transfection agent method. Panel (**c**) shows CD4 and CD62L expression at 4 hr postlabeling via electroporation.

T cell Quantification Using MRI

Using the in vivo ^{19}F MRI data we applied an algorithm (see Materials and Methods) to quantify the effective number of transferred cells within ROIs. Figure 4d shows a summary of the cell quantification results in pancreata from $n = 4$ animals. The number of apparent T cells detected ranged from ≈1.5–3.4% of the total transferred cells (Fig. 4d). The mean number of cells detected for the cohort was 2.2 ± 0.9% of the total transferred cells, where the uncertainty is the standard deviation ($n = 4$). The average cell density in vivo was ≈28,000 cells/voxel in the pancreas.

We independently validated the quantity of labeled cells homing to the pancreas via high-resolution ^{19}F NMR spectroscopy in excised organs (Fig. 5). The mouse was sacrificed after the MRI scan, and we harvested and fixed the pancreas and other organs. Figure 5a shows a ^{19}F NMR spectrum from an intact, excised pancreas. The area under the ^{19}F NMR peak of the pancreas, measured with respect to a TFA reference sample in the same NMR tube, gives the total ^{19}F content in the organ. In the pancreata, the mean number of cells detected for the cohort using NMR was 2.9 ± 0.3% of the total transferred cells, where the uncertainty is the standard deviation for $n = 4$. Thus, the mean cell numbers obtained by NMR in the excised organs is consistent with the values obtained using in vivo ^{19}F MRI. The excised spleens showed minimal ^{19}F NMR signal (Fig. 5b), as is seen in the MRI data.

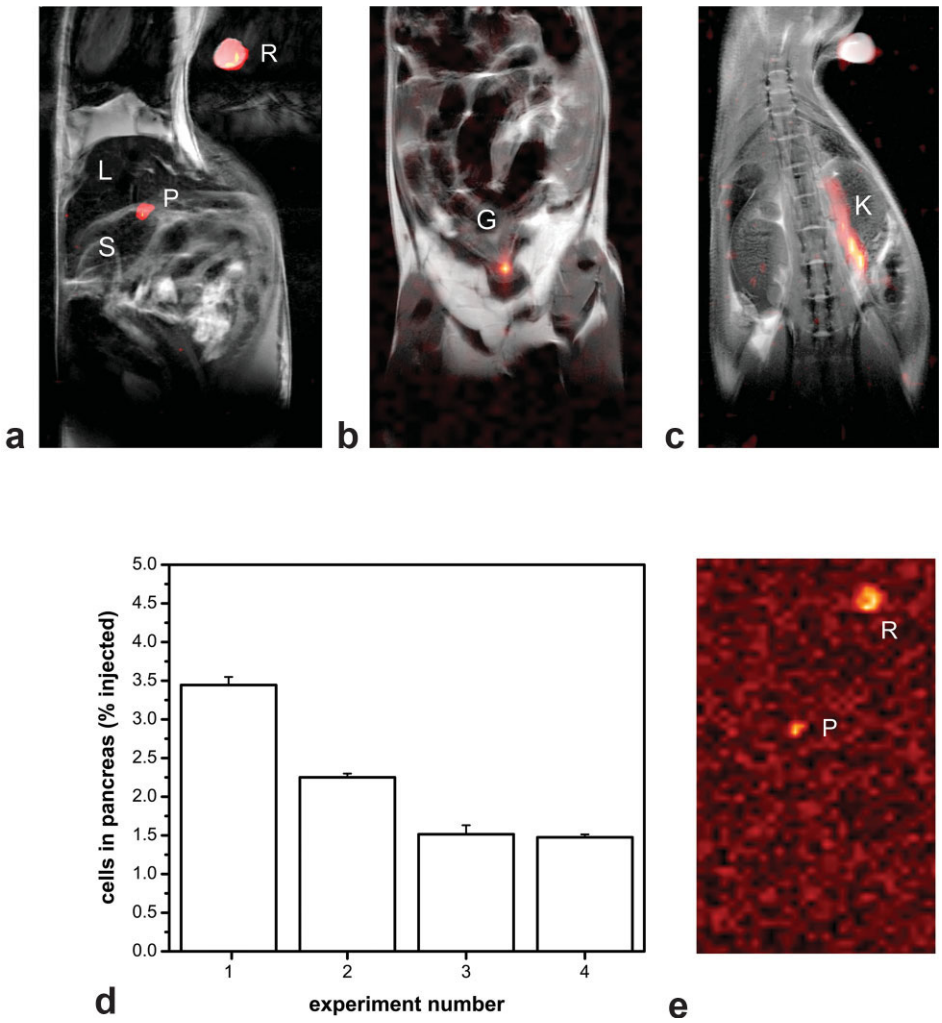

FIG. 4. In vivo MRI showing transferred T cells homing to the pancreas. Panels (**a–c**) are composite $^{19}F/^{1}H$ coronal images through the mouse torso, where the rostral direction is at the top of the panels. The ^{19}F is rendered in pseudo-color and the ^{1}H is in grayscale. Only slices containing ^{19}F signal are shown. (**a**) Image of PFPE-labeled, in vitro activated diabetogenic T cells (5×10^6) transferred i.p. into an NOD SCID mouse 48 hr prior. The image shows specific T cells (pseudo-color) homing to the pancreas (P). The ^{19}F reference capillary (R) is placed next to the mouse. The lungs, spleen (S), and liver (L) are labeled. (**b**) A negative control image of an NOD SCID mouse that received cell-free PFPE nanoparticles in PBS at an equivalent ^{19}F dose of 1×10^7 labeled T cells. We detected the PFPE (pseudo-color) only near the gut (G). The distributed, low-level signal in (**b**) is Johnson noise in these low SNR images. (**c**) A negative control image of a NOD SCID mouse that received activated, labeled MHC-mismatched T cells. We did not detect a signal in or around the pancreas, liver, or spleen, but cells (pseudo-color) can be seen at a site near the kidney (K). (**d**) Results of the in vivo quantification of the apparent T cells homing to the pancreas for the cohort of NOD SCID mice. The values represent the percentage of cells detected in the pancreas compared to the total number of i.p. transferred cells, ranging from 2–6 $\times$ 10^6 cells. See Materials and Methods for an explanation of error bars. (**e**) The raw, non-thresholded ^{19}F image from the same mouse as (**a**) showing the pancreas (P) and reference (R).

As an additional verification of the accuracy of the MRI cell quantification methods, we imaged a phantom containing a range of known densities of fixed, labeled T cells suspended in agarose. Figure 6a displays a composite $^{19}F/^{1}H$ image of the phantom; this image was acquired with the same parameters that were used for the in vivo data (Fig. 4a). In Fig. 6a, the chemical shift artifact (δ) from the CF_2 endgroup is seen from the highly concentrated R capillary. The SNR of R is 36.6, twice that of capillary A, and we do not see ghosts from the other capillaries after thresholding. Also, the R capillary contained a 4-fold higher concentration of fluorine than that used in the reference for the in vivo images. We calculated the number of apparent cells per voxel directly from the ^{19}F MR images using the same methods that were used for the in vivo data. The measured results are 120, 80, 43, 18, and 5.7 ($\times 10^3$) cells/voxel for capillaries A, B, C, D, and E, respectively (Fig. 6b). The Pearson correlation coefficient was 0.98 when compared to the actual cell numbers per voxel. Overall, the phantom experiment demonstrated reasonable accuracy of the quantitative methods, with a minimum cell detection limit of ≈7500 cells/voxel in vitro.

DISCUSSION

In this article we show that 'proxy' T cells can be efficiently labeled with PFPE nanoparticles ex vivo, enabling

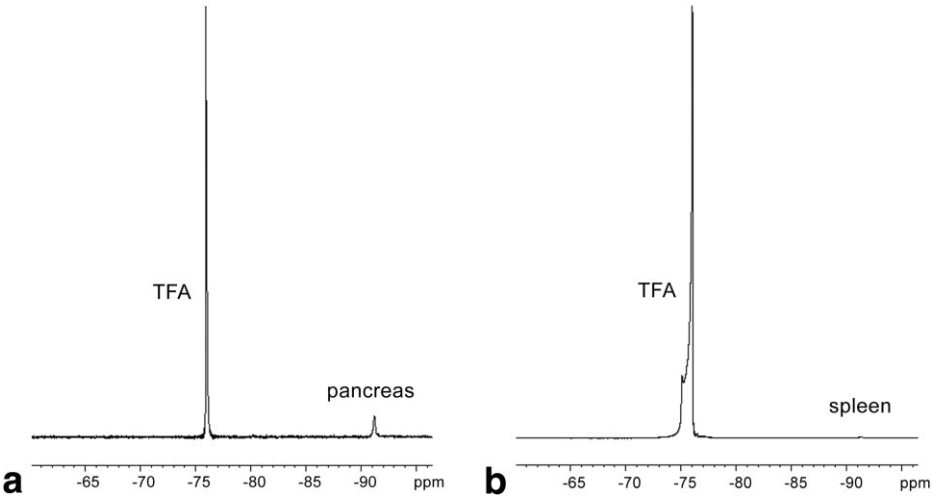

FIG. 5. ^{19}F NMR spectra of excised pancreas (**a**) and spleen (**b**) from an NOD SCID mouse inoculated with labeled T cells. ^{19}F NMR on whole, fixed organs was performed after in vivo MRI (Fig. 4a). The ^{19}F peak is detected in the pancreas (**a**), but is absent in the spleen (**b**), consistent with the in vivo MRI findings (Fig. 4a). The TFA ^{19}F reference was located in a sealed capillary adjacent the organ. A larger number of averages (8-times) were used to acquire (**b**) compared to (**a**).

visualization of selective homing and quantitation of inflammatory loci in vivo via ^{19}F MRI. For all in vivo experiments we used a well-established diabetes adoptive transfer model that has been shown to result in reproducible disease induction. This method maximizes the likelihood that the transferred cells will migrate to the pancreas within a short and reproducible time period. A quantitative image analysis method allowed us to determine that ≈2% of diabetogenic cells reached the pancreas 48 hr after cell transfer. High-resolution ^{19}F NMR in the excised pancreata validated the magnitude of cell counts. Histology of the pancreas confirmed selective homing of labeled T cells. Neither cell-free ^{19}F nanoparticles nor MHC-mismatched nonspecific T cells reached the pancreas at detectable levels, showing that only diabetogenic T cells were responsible for the observed ^{19}F signal. Importantly, we show that the PFPE nanoparticles are neither overtly cytotoxic nor stimulatory to T cells in vitro.

Several characteristics of PFPE nanoparticles make them useful as an intracellular MRI label for T cells and many other cell types. The carbon-fluorine bond is extremely stable, and most perfluorinated compounds are biologically inert. The PFPE is lipophobic and does not incorporate into cell membranes, nor will it degrade at typical lysosomal pH values. The ^{19}F NMR line shape and chemical shift of PFPE is not altered within cells, implying that

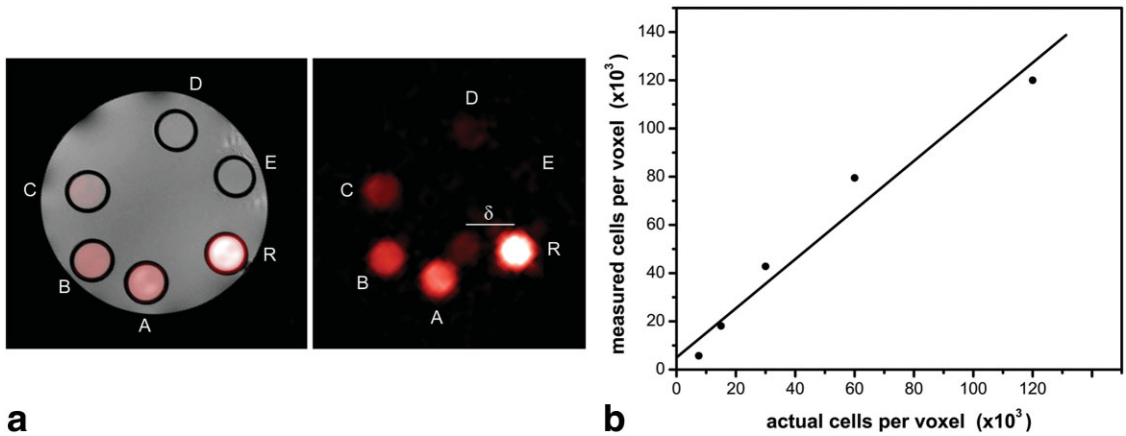

FIG. 6. Phantom studies validating T-cell quantification methods using ^{19}F MR images. (**a**) A composite $^{19}F/^{1}H$ image (left) and intensity-rescaled ^{19}F image (right) through a phantom containing capillary tubes containing different densities of labeled T cells suspended in agarose, where capillary A = 12, B = 6, C = 3, D = 1.5, and E = 0.75 ($\times 10^4$) cells/voxel, and R is a calibrated ^{19}F reference capillary. The ^{19}F image (**a**, right) was rescaled to show the intermediate cell densities, i.e., capillaries B, C, D. Capillary E (7500 cells/voxel) is not visible in this scaling; however, our quantitative analysis is able to detect and measure cells in this sample. In (**a**), the chemical shift artifact (δ) from the CF_2 endgroup is seen from the highly concentrated R capillary. These data were acquired using similar imaging parameters as Fig. 4. (**b**) The actual versus MRI-measured cell numbers in the phantom. The Pearson correlation coefficient is 0.98. The linear fit is a guide for the eye. The error bars for the ordinate are not shown and are smaller than the data point symbol.

the compound is not significantly metabolized. ^{19}F has low background biological abundance and is a sensitive nucleus, where the gyromagnetic ratios of ^{1}H and ^{19}F differ by only about 6%, and the relative sensitivity is 0.83. Previously, ^{19}F MRI and perfluorocarbons have been used for several extracellular applications, including blood volume measurements (24), measurements of tissue oxygenation (25–32), and the detection of atherosclerotic plaques (33,34).

Previously, dendritic cells have been labeled for in vivo MRI using a perfluoro-15-crown-5-ether molecule (18). In the present experiments we chose a linear PFPE molecule having a larger number of ^{19}F atoms per molecule for high sensitivity. For the linear PFPE, the chemical-shifted ^{19}F spins from the end groups are below the detection limit in our in vivo MRI acquisitions and has ≈0.1 lower intensity than the main peak. Thus, with in vivo SNR-values the CF_2 endgroup is never observed. In addition, the T1 of this molecule is a factor of 2.2 shorter T_1 at 11.7T (in air) compared to the perfluoro-15-crown-5-ether, thus permitting shorter imaging times. The linear PFPE does not readily coordinate O_2 as does the perfluoro-15-crown-5-ether, and hence it is less sensitive to T_1 changes due to local differences in the partial pressure of O_2 (pO_2).

Using confocal microscopy, we observed that fluorescently labeled PFPE nanoparticles appear bound to the cell membrane or localized within cells (Fig. 1b). These data, along with the observation via flow cytometry of a transient decrease in CD4 expression (Fig. 2b) suggests a possible receptor-mediated endocytosis (RME) uptake mechanism when using transfection agents. CD4 is known to localize to clathrin-coated pits, and reduced CD4 expression has been shown to occur during RME (35). To test this hypothesis, cells were labeled using an alternative technique without transfection agent. Labeling through electroporation, which results in comparable loading per cell (data not shown), does not affect CD4 levels (Fig. 2c). This suggests that the transient downregulation of CD4 only occurs when the particles are taken up by the cells in the presence of transfection agent, rather than due to any biological effect of the PFPE itself. Importantly, this temporary CD4 downregulation did not appear to affect cell function in vivo, as the cells were still able to traffic to the pancreas in a reasonable time frame.

The NOD mouse has been studied for over 20 years as a model of human T1D. It shares many of the genetic and immunological features of the human disease, including the presence of diabetogenic T cells and spontaneous development of diabetes. The T1D model using adoptive transfer of NOD BDC2.5 T cells is well established (22,36). $CD4^+$ T cells play a key role in diabetogenesis, and their ability to cause diabetes in adult NOD SCID mice is accelerated when the mice are pretreated with cyclophosphamide (20), and this allowed us to observe infiltrating T cells at an early and predictable time after injection. Activated BDC2.5 T cells of both Th1 and Th2 type can rapidly induce diabetes in NOD SCID (22,37). This model, although artificial, created a useful platform for optimizing the quantitative aspects of these techniques.

The cell trafficking pattern we observed is consistent with similar studies in NOD mice, including those using fluorescently labeled T cells (23) and SPIO-labeled diabetogenic T cells (11). We observed on the order of ≈2% of labeled transferred T cells in the pancreas using the MRI data. We note that this small number of observed cells is consistent with a related study by Fabien et al. (38) that used FACS analysis on excised tissue. In control experiments nonfunctional cells were injected into the intraperitoneal cavity on one side of the mouse. The cells in Fig. 4c are likely inside the i.p. cavity near the kidney on one side. The actual location of these cells has no biological significance other than they were not found in the pancreas. These MHC-mismatched cells were nonfunctional and thus would eventually undergo apoptosis.

The majority of transferred cells are at concentrations too low to be detected in lymph nodes or other tissues by MRI, remain in circulation, or are distributed within the i.p. cavity. Cells in circulation will not be detected using this technique. The total amount of PFPE delivered to the subject, contained within the autoreactive T cells, is only a trace amount (0.1 g/kg), and thus it is only detected when a sufficient number of ^{19}F spins (i.e., labeled cells) accumulate in a given voxel above a detection threshold. In previous reports (18) we injected PFPE-labeled dendritic cells (DCs) intravenously into mice. In these experiments we clearly detected ^{19}F in the liver and spleen using similar in vivo MRI methods. In the present experiments we did not detect ^{19}F in these organs. The absence of signal in the spleen in liver is a good indicator that the T cells have not died and are in circulation and/or present in tissues at concentrations below detectability.

An approximate theoretical analysis of the practical detection limitations of the number of ^{19}F spins and PFPE-labeled cells per voxel using a typical clinical scanner is given elsewhere (18). Our phantom studies show that we are able to detect >7500 cells/voxel using the same in vivo imaging parameters; the cell densities (per voxel) reported in vivo are ≈4-times higher than this value. With further refinements in sequence design and cell labeling techniques, we believe that the cell detection limits can be improved several-fold, and this is under investigation. Single cell imaging is not possible with the PFPE approach, as has been reported by several groups using SPIO agents. The ultimate sensitivity of the PFPE technique is not known and certainly depends on many technical details of the subject and the imaging system used.

For cell count calculations we used signals measured from the MRI datasets. Noise in complex images is normally distributed about zero independently for both the real and imaginary components in each voxel. Because the ^{19}F images are in the low SNR regime, converting the complex-valued images to magnitude images, which is commonplace in conventional MRI, creates non-normally distributed noise with a Rician distribution (21). Consequently, magnitude images have a nonzero mean pixel value in regions devoid of signal, which introduces a noise-dependent bias to the data. Our analysis compensates for the Rician bias by rescaling magnitude intensity values that are close to zero.

Several factors may potentially diminish the MRI cell quantification accuracy in vivo. We assume that the amount of ^{19}F per cell (F_c) is a constant. However, F_c will decrease by 1/2 with each cell division. Imaging was carried out 48 hr after cell transfer in order to provide suffi-

cient time for homing. Although the actual division rate of our T cells in vivo is unknown, the doubling time should be at least 1.5 days based on previous results (39,40). A lack of precise determination of the cell division rate may contribute to uncertainty in quantification, but this is unlikely to affect the values by more than a factor of two. Even though the PFPE is not degraded by the cell, loss of label (e.g., by exocytosis) is another consideration that could, in principle, lead to an underestimation of cell numbers. However, preliminary in vitro studies have shown that the label is retained in T cells for at least 18 hr. Other studies in DCs have shown that similar labels are retained for over 5 days (18). Additionally, PFPE nanoparticles may be taken up by resident cells, such as macrophages, if cell lysis occurs, thereby releasing the nanoparticles, or if the T cell is endocytosed. However, this will only affect quantification accuracy if significant numbers of these phagocytes remain localized within an ROI. Furthermore, the apparent absence of MRI signal in the liver and spleen is noteworthy because it implies that significant numbers of transferred cells likely did not die.

CONCLUSION

In this article we have demonstrated a novel noninvasive imaging method to visualize and quantify specific immune cell homing behavior in an adoptive transfer model of an autoimmune disease. A distinctive feature of our approach is that the images created have exquisite specificity for the labeled cells. Furthermore, this approach yields reliable estimates of the apparent number of cells from image data, thus providing a unique in vivo biomarker. This technology in its present form can be used to investigate detailed biological questions concerning the trafficking of inflammatory cells in vivo.

ACKNOWLEDGMENTS

We thank Jelena M. Janjic, Deepak Kumar Kana Kadayakkara, Kevin Hitchens, Virgil Simplaceanu, Dewayne Falkner, and Chris Navara for valuable assistance.

REFERENCES

1. Miyazaki A, Hanafusa T, Yamada K, Miyagawa J, Fujinokurihara H, Nakajima H, Nonaka K, Tarui S. Predominance of lymphocytes-T in pancreatic-islets and spleen of pre-diabetic non-obese diabetic (NOD) mice — a longitudinal-study. Clin Exp Immunol 1985;60:622–630.
2. Leiter EH, Prochazka M, Coleman DL. The nonobese diabetic (NOD) mouse. Am J Pathol 1987;128:380–383.
3. Yeh TC, Zhang W, Ildstad ST, Ho C. Intracellular labeling of T-cells with superparamagnetic contrast agents. Magn Reson Med 1993;30: 617–625.
4. Lewin M, Carlesso N, Tung CH, Tang XW, Cory D, Scadden DT, Weissleder R. Tat peptide-derivatized magnetic nanoparticles allow in vivo tracking and recovery of progenitor cells. Nat Biotechnol 2000;18: 410–414.
5. Hoehn M, Kustermann E, Blunk J, Wiedermann D, Trapp T, Wecker S, Focking M, Arnold H, Hescheler J, Fleischmann BK, Schwindt W, Buhrle C. Monitoring of implanted stem cell migration in vivo: A highly resolved in vivo magnetic resonance imaging investigation of experimental stroke in rat. Proc Natl Acad Sci U S A 2002;99:16267–16272.
6. Ahrens ET, Feili-Hariri M, Xu H, Genove G, Morel PA. Receptor-mediated endocytosis of iron-oxide particles provides efficient labeling of dendritic cells for in vivo MR imaging. Magn Reson Med 2003;49: 1006–1013.
7. Kircher MF, Allport JR, Graves EE, Love V, Josephson L, Lichtman AH, Weissleder R. In vivo high resolution three-dimensional imaging of antigen-specific cytotoxic T-lymphocyte trafficking to tumors. Cancer Res 2003;63:6838–6846.
8. Bulte JWM, Arbab AS, Douglas T, Frank JA. Preparation of magnetically labeled cells for cell tracking by magnetic resonance imaging. Method Enzymol 2004;386:275–299.
9. Modo M, Mellodew K, Cash D, Fraser SE, Meade TJ, Price J, Williams SCR. Mapping transplanted stem cell migration after a stroke: a serial, in vivo magnetic resonance imaging study. Neuroimage 2004;21:311–317.
10. Billotey C, Aspord C, Beuf O, Piaggio E, Gazeau F, Janier MF, Thivolet C. T-cell homing to the pancreas in autoimmune mouse models of diabetes: in vivo MR imaging. Radiology 2005;236:579–587.
11. Moore A, Grimm J, Han B, Santamaria P. Tracking the recruitment of diabetogenic CD8+ T-cells to the pancreas in real time. Diabetes 2004; 53:1459–1466.
12. Anderson SA, Shukaliak-Quandt J, Jordan EK, Arbab AS, Martin R, McFarland H, Frank JA. Magnetic resonance imaging of labeled T-cells in a mouse model of multiple sclerosis. Ann Neurol 2004;55:654–659.
13. Evgenov NV, Medarova Z, Pratt J, Pantazopoulos P, Leyting S, Bonner-Weir S, Moore A. In vivo imaging of immune rejection in transplanted pancreatic islets. Diabetes 2006;55:2419–2428.
14. Evgenov NV, Medarova Z, Dai GP, Bonner-Weir S, Moore A. In vivo imaging of islet transplantation. Nat Med 2006;12:144–148.
15. Turvey SE, Swart E, Denis MC, Mahmood U, Benoist C, Weissleder R, Mathis D. Noninvasive imaging of pancreatic inflammation and its reversal in type 1 diabetes. J Clin Invest 2005;115:2454–2461.
16. Wu YL, Ye Q, Foley LM, Hitchens TK, Sato K, Williams JB, Ho C. In situ labeling of immune cells with iron oxide particles: An approach to detect organ rejection by cellular MRI. Proc Natl Acad Sci U S A 2006;103:1852–1857.
17. Shapiro EM, Sharer K, Skrtic S, Koretsky AP. In vivo detection of single cells by MRI. Magn Reson Med 2006;55:242–249.
18. Ahrens ET, Flores R, Xu H, Morel PA. In vivo imaging platform for tracking immunotherapeutic cells. Nat Biotechnol 2005;23:983–987.
19. You S, Chen C, Lee WH, Wu CH, Judkowski V, Pinilla C, Wilson DB, Liu CP. Detection and characterization of T cells specific for BDC2.5 T cell-stimulating peptides. J Immunol 2003;170:4011–4020.
20. Ablamunits V, Quintana F, Reshef T, Elias D, Cohen IR. Acceleration of autoimmune diabetes by cyclophosphamide is associated with an enhanced IFN-gamma secretion pathway. J Autoimmun 1999;13:383–392.
21. Gudbjartsson H, Patz S. The Rician distribution of noisy MRI data. Magn Reson Med 1995;34:910–914.
22. Cantor J, Haskins K. Effector function of diabetogenic CD4 Th1 T cell clones: a central role for TNF-alpha. J Immunol 2005;175:7738–7745.
23. Phillips JM HS, Parish NM, Fehervari Z, Haskins K, Cooke A. Nondepleting anti-CD4 has an immediate action on diabetogenic effector cells, halting their destruction of pancreatic beta cells. J Immunol 2000;165:1949–1955.
24. Meyer KL, Joseph PM, Mukherji B, Livolsi VA, Lin R. Measurement of vascular volume in experimental rat tumors by 19F magnetic resonance imaging. Invest Radiol 1993;28:710–719.
25. Fishman JE, Joseph PM, Floyd TF, Mukherji B, Sloviter HA. Oxygen-sensitive 19F NMR imaging of the vascular system in vivo. Magn Reson Imaging 1987;5:279–285.
26. Eidelberg D, Johnson G, Barnes D, Tofts PS, Delpy D, Plummer D, McDonald WI. 19F NMR imaging of blood oxygenation in the brain. Magn Reson Med 1988;6:344–352.
27. McGoron AJ, Pratt R, Zhang J, Shiferaw Y, Thomas S, Millard R. Perfluorocarbon distribution to liver, lung and spleen of emulsions of perfluorotributylamine (FTBA) in pigs and rats and perfluorooctyl bromide (PFOB) in rats and dogs by 19F NMR spectroscopy. Artif Cells Blood Sub 1994;22:1243–1250.
28. Dardzinski BJ, Sotak CH. Rapid tissue oxygen tension mapping using 19F inversion-recovery echo-planar imaging of perfluoro-15-crown-5-ether. Magn Reson Med 1994;32:88–97.
29. Noth U, Morrissey SP, Deichmann R, Adolf H, Schwarzbauer C, Lutz J, Haase A. In vivo measurement of partial oxygen pressure in large vessels and in the reticuloendothelial system using fast 19F-MRI. Magn Reson Med 1995;34:738–745.
30. Lutz J, Noth U, Morrissey SP, Adolf H, Deichmann R, Haase A. Measurement of oxygen tensions in the abdominal cavity and in the skeletal muscle using 19F-MRI of neat PFC droplets. Adv Exp Med Biol 1997;428:569–572.

31. Sotak CH, Hees PS, Huang HN, Hung MH, Krespan CG, Raynolds S. A new perfluorocarbon for use in fluorine-19 magnetic resonance imaging and spectroscopy. Magn Reson Med 1993;29:188–195.
32. Xia MN, Kodibagkar V, Liu HL, Mason RP. Tumour oxygen dynamics measured simultaneously by near-infrared spectroscopy and F-19 magnetic resonance imaging in rats. Phys Med Biol 2006;51:45–60.
33. Morawski AM, Winter PM, Yu X, Fuhrhop RW, Scott MJ, Hockett F, Robertson JD, Gaffney PJ, Lanza GM, Wickline SA. Quantitative "magnetic resonance immunohistochemistry" with ligand-targeted F-19 nanoparticles. Magn Reson Med 2004;52:1255–1262.
34. Lanza GM, Winter PM, Neubauer AM, Caruthers SD, Hockett FD, Wickline SA. 1H/19F magnetic resonance molecular imaging with perfluorocarbon nanoparticles. In: Ahrens ET, editor. In vivo cellular and molecular imaging. Vol. 70. Current topics in developmental biology. San Diego: Elsevier; 2005. p 58–78.
35. Pelchen-Matthews A, Parsons IJ, Marsh M. Phorbol ester-induced downregulation of CD4 is a multistep process involving dissociation from p56lck, increased association with clathrin-coated pits, and altered endosomal sorting. J Exp Med 1993;178:1209–1222.
36. Phillips JM, Haskins K, Cooke A. MAdCAM-1 is needed for diabetes development mediated by the T cell clone, BDC-2.5. Immunology 2005;116:525–531.
37. Pakala SV, Kurrer MO, Katz JD. T helper 2 (Th2) T cells induce acute pancreatitis and diabetes in immune-compromised nonobese diabetic (NOD) mice. J Exp Med 1997;186:299–306.
38. Fabien N, Bergerot I, Maguer-Satta V, Orgiazzi J, Thivolet C. Pancreatic lymph nodes are early targets of T cells during adoptive transfer of diabetes in NOD mice. J Autoimmun 1995;8:323–334.
39. Miller MJ, Safrina O, Parker I, Cahalan MD. Imaging the single cell dynamics of CD4+ T cell activation by dendritic cells in lymph nodes. J Exp Med 2004;200:847–856.
40. Ribeiro RM, Mohri H, Ho DD, Perelson AS. In vivo dynamics of T cell activation, proliferation, and death in HIV-1 infection: why are CD4+ but not CD8+ T cells depleted? Proc Natl Acad Sci U S A 2002;99:15572–15577.